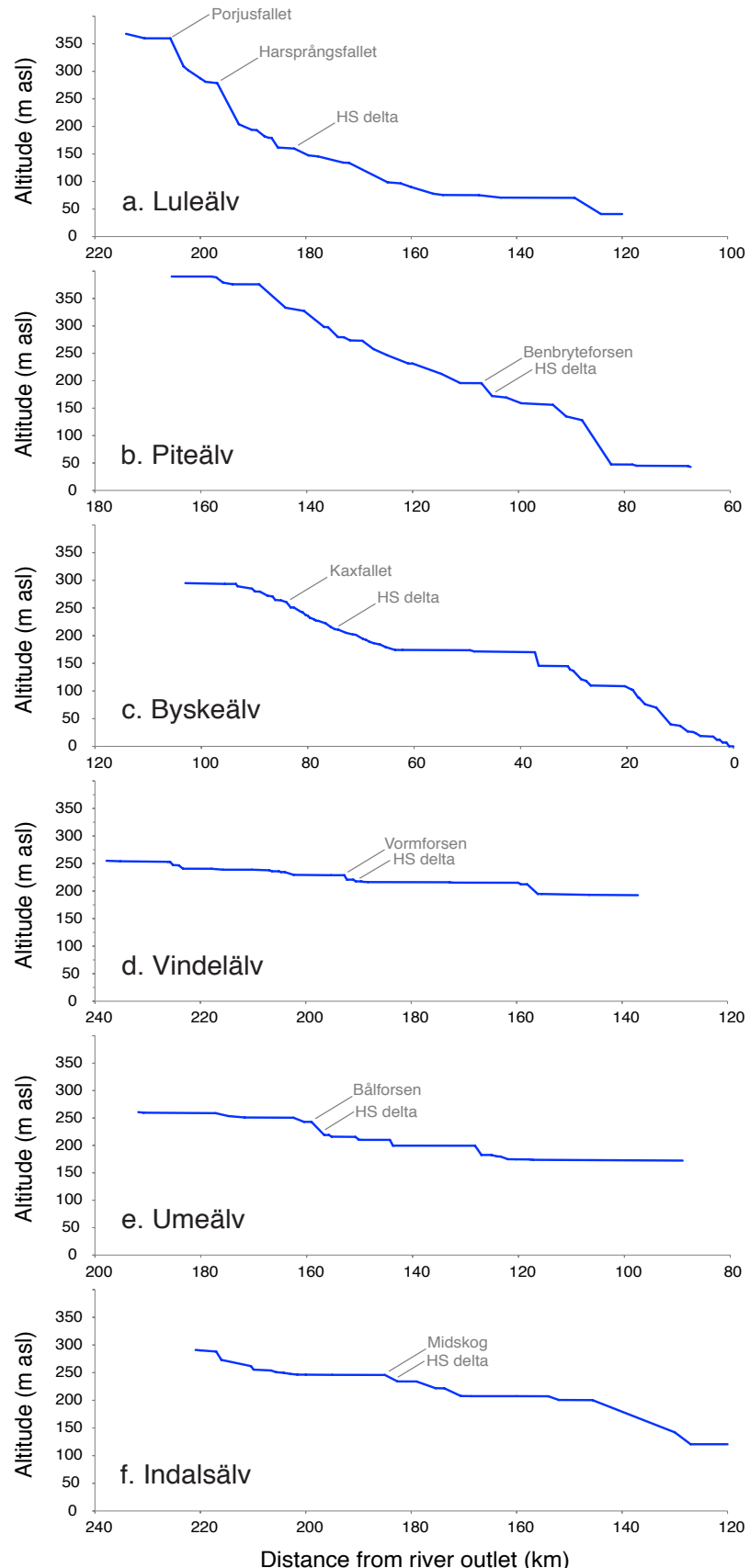
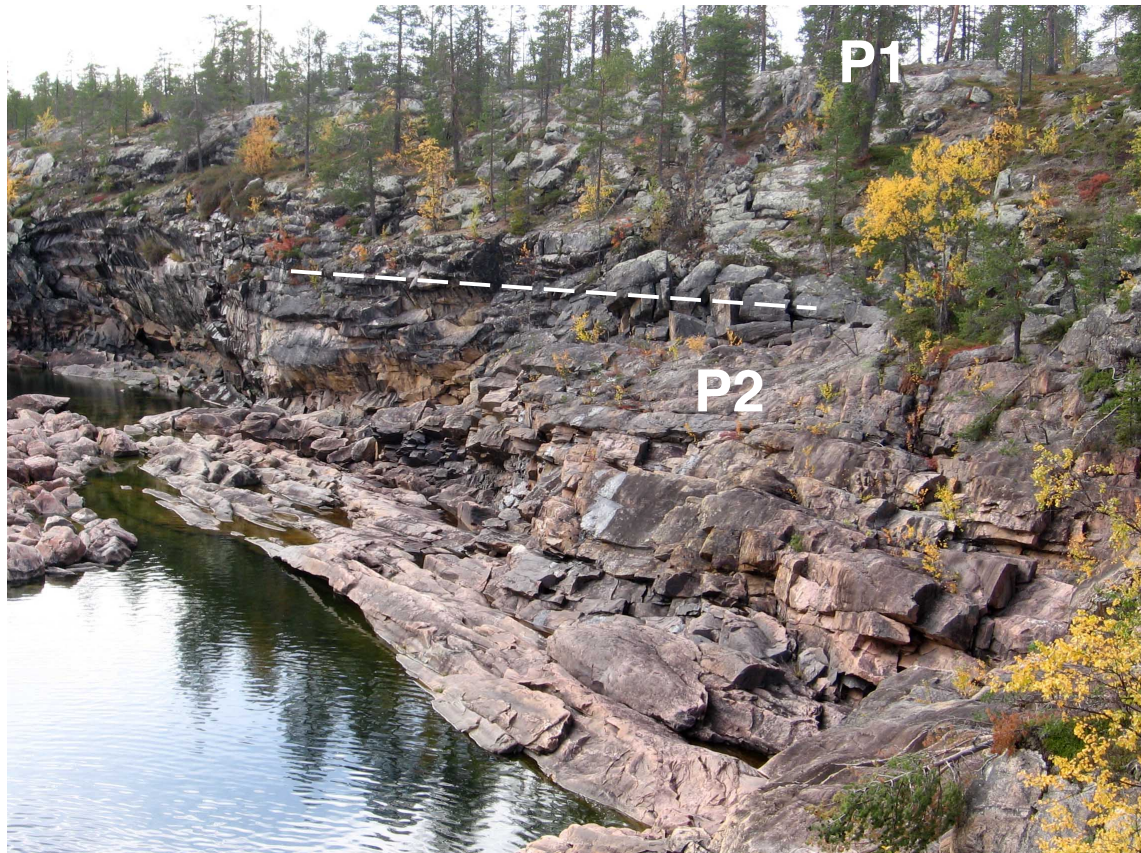


## SUPPLEMENTARY INFORMATION



**Supplementary Figure 1. River long profiles.** These are derived from pre-dam field surveys<sup>3</sup>. 'HS delta' marks the apex of the highest shoreline glaciofluvial delta in each valley.



**Supplementary Figure 2.** Porjusfallet gorge wall (~24 m high) sampled for exposure dating (Fig. 2a, samples P1, P2). The zone of active bedrock channel erosion is indicated (white dashes); the low water-level is due to the dam just upstream.



**Supplementary Figure 3.** Porjusfallet upper surface sampled for exposure dating (Fig. 2a, sample P1). Note streamlined bedrock forms.



**Supplementary Figure 4.** Harsprånget gorge overview (~35 m deep, Fig. 2b); this location is ~1.3 km downstream of Harsprångsfallet shown in Fig. S2.13. The low water level is due to the dam upstream.



**Supplementary Figure 5.** Harsprången gorge wall surface sampled for exposure dating (Fig. 2b, sample H4).



**Supplementary Figure 6.** Harsprånget upper surface sampled for exposure dating (Fig. 2b, sample H1).



**Supplementary Figure 7.** Benbryteforsen gorge—zone of active bedrock channel erosion (below white dashes; Fig. 2c).



**Supplementary Figure 8.** Benbryteforsen upper surface sampled for exposure dating (Fig. 2c, sample B2). Note streamlined bedrock forms.



**Supplementary Figure 9.** Kaxfallet gorge—zone of active bedrock channel erosion (below white dashes; Fig. 2d). The upper surface sampled for exposure dating forms visible skyline.



**Supplementary Figure 10.** Vormforsen surface sampled for exposure dating (Fig. 2e, sample V1).



**Supplementary Figure 11.** Bålforseñ gorge sampled for exposure dating (Fig. 2f, samples U1, U2). The zone of active bedrock channel erosion is indicated (white dashes); the low water-level is due to the dam just upstream (spillway at right).



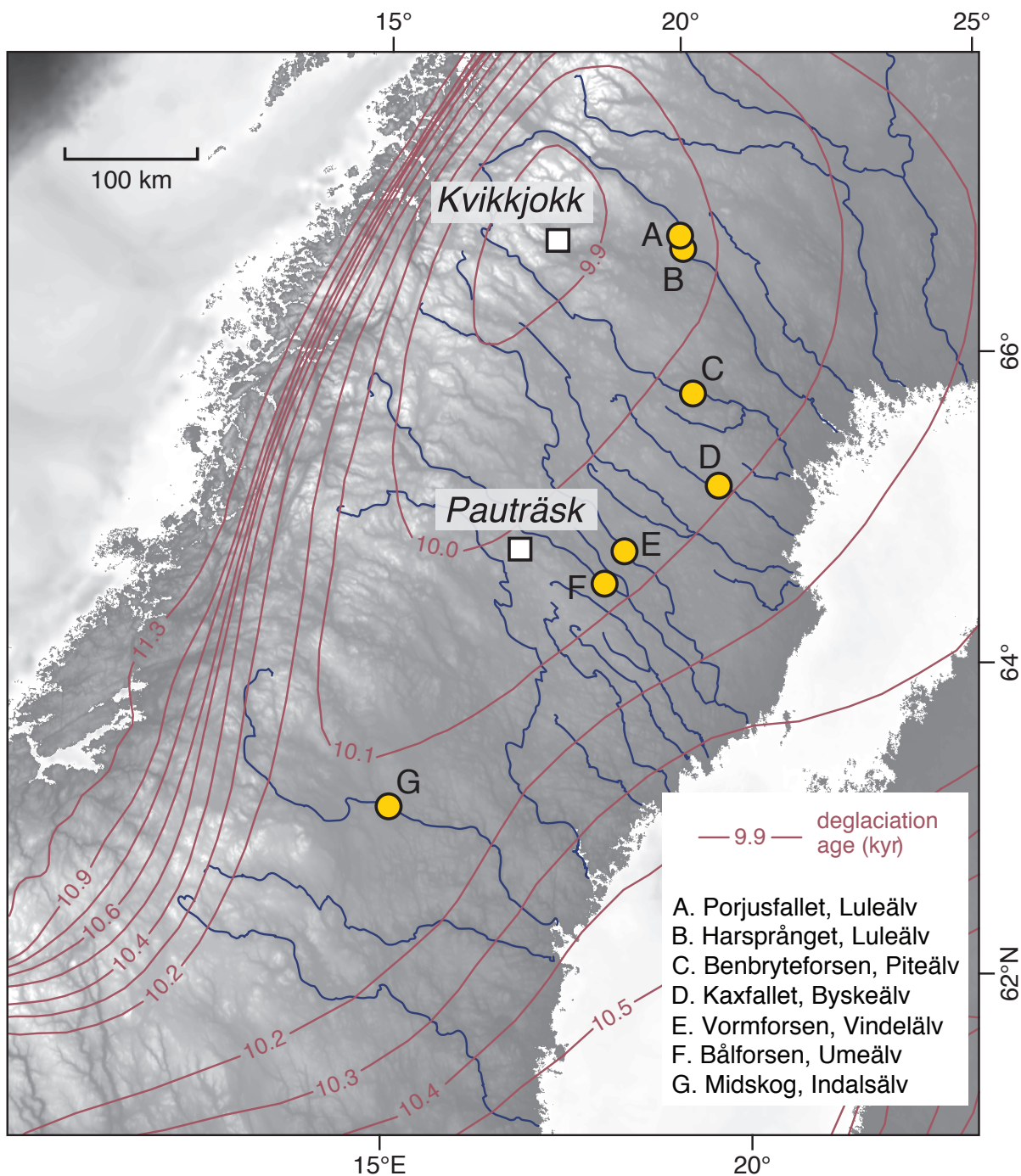
**Supplementary Figure 12.** Midskog channel bed sampled for exposure dating (Fig. 2g, sample M1). Access to the channel bed is possible due to the dam just upstream.



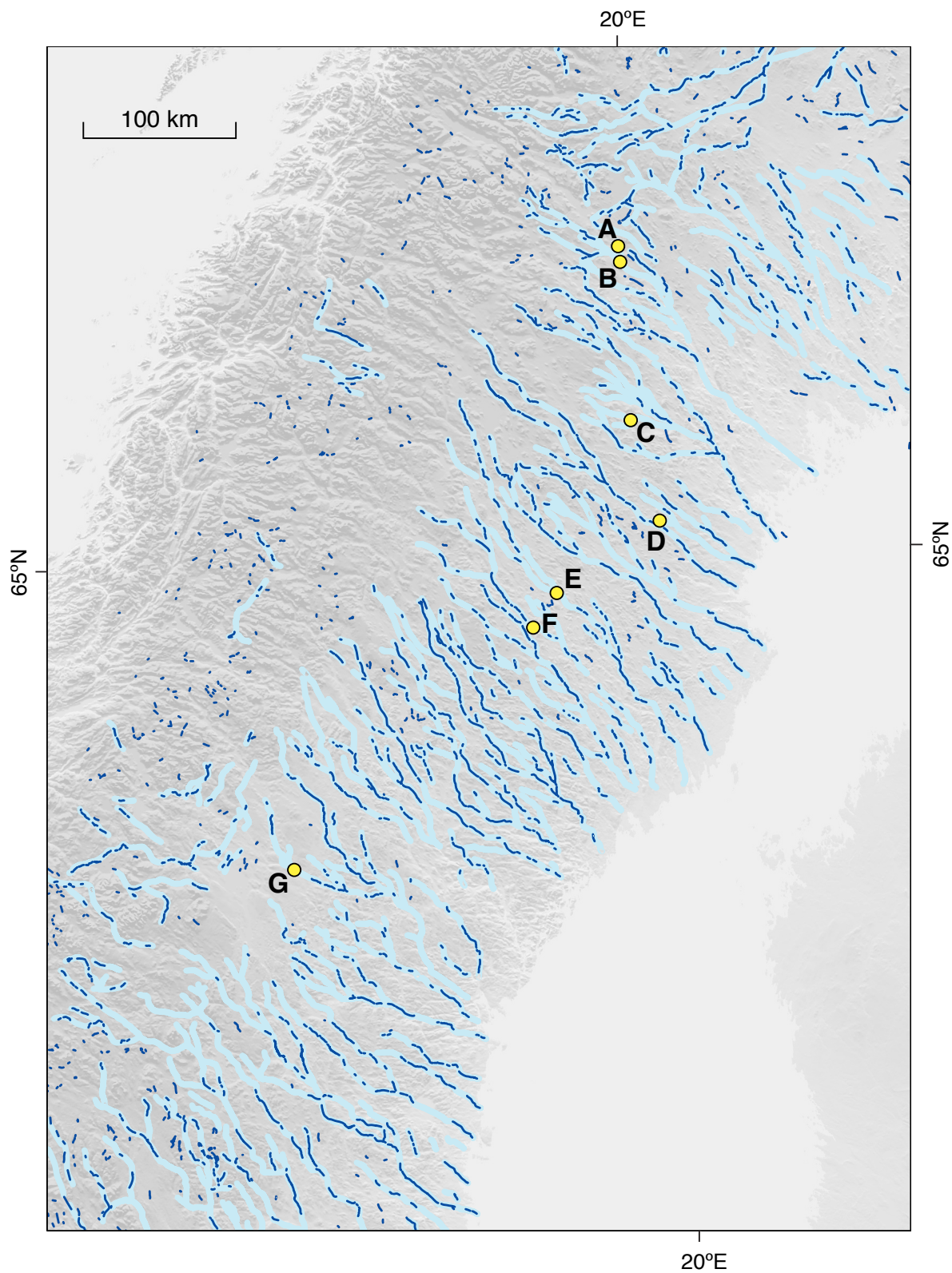
**Supplementary Figure 13.** Harsprångsfallet, Luleälv, before and after the hydro-electric dam was constructed in the 1950s (left, photographer unknown; right, photograph by J.D. Jansen).



**Supplementary Figure 14.** Chromolithograph by Carl Svante Hallbeck (1856) depicting Harsprångsfallet (known by its Sámi name: Njommelsaska) illuminated by the aurora borealis in the polar night. Despite having the appearance of a highly erosive fluvial environment, this steep gorge emerged virtually fully-formed from under the retreating ice sheet at ~10 kyr, and has subsequently undergone just a few metres of bedrock incision. This image is in the public domain.



**Supplementary Figure 15. Deglaciation isochrons** (red, in kyr) showing the ice-margin retreat post-Younger Dryas (identical to Fig. 1A). Pauträsk ( $64.81^{\circ}$  N,  $17.52^{\circ}$  E) is the northwesternmost locality linked to the Swedish clay-varve chronology<sup>1</sup>, and the Kvikkjokk area is where the final ice remnants vanished. Also shown are the 7 inner gorges sampled for exposure dating (yellow dots labelled A to G).



**Supplementary Figure 16. Eskers & subglacial drainage paths.** Spatial distribution of eskers, i.e., ridges of glaciofluvial material (dark blue lines), after Hättestrand (1998)<sup>2</sup>, and the 7 inner gorges sampled for exposure dating (yellow dots labelled A to G). Reconstructed subglacial drainage paths are indicated (thick light-blue lines) by linking esker segments according to other signs of subglacial meltwater drainage, such as channels and glaciofluvial sediments of more diffuse morphology. Note that for sites examined in this study, the subglacial drainage paths closely follow present-day river systems (Supplementary Fig. 1).

**Supplementary Table 1. Sites sampled for  $^{10}\text{Be}$  exposure dating.**

Site, river	Location (decimal deg.)	Highest shoreline altitude (m a.s.l.)	Drainage area ( $\text{km}^2$ )	Annual peak discharge ( $\text{m}^3/\text{s}$ )
A. Porjusfallet, Luleälv	66.956 N, 19.790 E	170–165	10,020	600
B. Harsprånget, Luleälv	66.867 N, 19.817 E	170–165	10,020	605
C. Benbryteforsen, Piteälv	65.906 N, 19.982 E	177–174	6,780	445
D. Kaxfallet, Byskeälv	64.870 N, 18.723 E	220–215	3,120	190
E. Vormforsen, Vindelälv	65.320 N, 20.125 E	~224	9,010	565
F. Bålforsten, Umeälv	64.654 N, 18.487 E	225–222	11,840	710
G. Midskog, Indalsälv	63.241 N, 15.242 E	230–225	18,850	1,040

Drainage area (A) and discharge (Q) pertain to rivers at the highest shorelines; average annual peak discharge calculated via regression analysis of regional flow gauge data:  $Q=0.29A^{0.83}$  (based on data in ref.4).

**Supplementary Table 2. Summary of inner gorge  $^{10}\text{Be}$  analyses.**

Sample ID <sup>a</sup>	River	Latitude (deg.)	Longitude (deg.)	Altitude <sup>b</sup> (m a.s.l.)	Thick. <sup>c</sup> (cm)	Topo. Shielding <sup>d</sup>	$^{10}\text{Be}$ Conc. <sup>e</sup> (atoms/g)	$^{10}\text{Be}$ Unc. <sup>f,g</sup> (atoms/g)	Be AMS Standard <sup>h</sup>	AMS Lab.	$^{10}\text{Be}$ Age <sup>i</sup> (yr)	$^{10}\text{Be}$ Age Internal Unc. <sup>j</sup> (yr)	$^{10}\text{Be}$ Age External Unc. <sup>j</sup> (yr)
P1	Luleälv	66.9564	19.7888	353.0	2.0	0.9999	55798	3081	S2007N	ETH	8850	490	585
P1*	Luleälv	66.9564	19.7888	353.0	2.0	0.9999	54991	3518	S2007N	ETH	8722	559	642
P2	Luleälv	66.9563	19.7903	337.9	2.0	0.9779	58860	6888	S2007N	ETH	9681	1136	1189
P2*	Luleälv	66.9563	19.7903	337.9	2.0	0.9779	60367	2974	S2007N	ETH	9930	490	608
H1	Luleälv	66.8670	19.8217	266.2	1.0	0.9998	48448	3280	S2007N	ETH	8300	563	638
H2	Luleälv	66.8669	19.8190	257.4	1.0	0.9998	51910	3440	S2007N	ETH	8973	596	679
H3	Luleälv	66.8668	19.8182	253.4	1.0	0.9997	59167	3032	S2007N	ETH	10273	528	646
H4	Luleälv	66.8667	19.8177	246.5	1.5	0.9945	50698	3102	S2007N	ETH	8941	548	637
H5	Luleälv	66.8672	19.8174	234.4	2.0	0.9842	57319	3681	S2007N	ETH	10382	668	767
B1	Piteälv	65.9048	19.9802	204.7	2.0	0.9997	120534	4716	NIST_30600	SUERC	20327	799	1088
B2	Piteälv	65.9055	19.9823	198.9	2.0	0.9999	66478	4388	NIST_30600	SUERC	11249	745	849
K1	Byskeälv	65.3196	20.1246	266.5	1.5	0.9999	99799	7767	NIST_30600	SUERC	15750	1231	1357
V1	Vindelälv	64.8704	18.7235	237.7	1.0	0.9999	60246	4695	NIST_30600	SUERC	9744	761	839
U1	Umeälv	64.6540	18.4866	234.7	2.0	0.9997	86005	4485	S2007N	ETH	15442	808	984
U2	Umeälv	64.6544	18.4874	229.8	2.0	0.9994	51015	2732	S2007N	ETH	9193	493	595
M1	Indalsälv	63.2414	15.2392	229.6	2.0	0.9998	46301	3139	S2007N	ETH	8384	570	645
M2	Indalsälv	63.2409	15.2416	228.1	2.0	0.9998	59426	5063	S2007N	ETH	10783	921	1001

a. Duplicate measurements (i.e., two separate aliquots measured from the same sample) are denoted by \*.

b. Sample altitude measured via differential global positioning system ( $\pm 1\sigma$  height uncertainty <10 cm).

c. The tops of all samples were exposed at the surface, and to minimise likelihood of shielding by overburden each sample comprises up to 20 amalgamated sub-samples from the surrounding surface (vertical range <1 m for all sub-samples). Age modelling assumes zero rock surface erosion and zero shielding since exposure.

d. Calculated according to ref.5 based on data collected in the field.

e. Concentrations (Conc.) are corrected for a full chemistry procedural blank that yielded <3% of the number of  $^{10}\text{Be}$  atoms in the samples.

f. Uncertainties (Unc.) are reported at  $1\sigma$  confidence level.

g. Propagated uncertainties include error in the blank, carrier mass (2%), and counting statistics.

h. CRONUS-Earth online calculator nomenclature. S2007N (equivalent to 07KNSTD) has  $^{10}\text{Be}/^{9}\text{Be}$  isotope ratio of  $28.1 \times 10^{-12}$  (ref.6) and is consistent with  $^{10}\text{Be}$  half-life of  $1.387 \pm 0.012$  Myr (refs 7–9). NIST\_30600 has  $^{10}\text{Be}/^{9}\text{Be}$  isotope ratio of  $3.06 \times 10^{-11}$  (ref.10) and is consistent with  $^{10}\text{Be}$  half-life of 1.51 Myr (refs 11–13). All  $^{10}\text{Be}$  concentrations are renormalized to standard 07KNSTD during exposure age calculations such that all results are consistent with the updated  $^{10}\text{Be}$  half-life of  $1.387 \pm 0.012$  Myr.

i. Calculated using CRONUS-Earth online calculator source code version 2.2 (ref.14) (<http://hess.ess.washington.edu/>) constants file 2.2.1 with updated reference spallation production rates (ref.15), using the time-dependent Lal/Stone scaling scheme (reference spallation production rate  $4.15 \pm 0.15$  atoms g $^{-1}$  yr $^{-1}$ ). Calculations assume density of  $2.7 \text{ g cm}^{-3}$ .

j. Internal uncertainty accounts for the analytical uncertainty associated with measuring  $^{10}\text{Be}$  concentrations. Propagated errors in the model ages represent external uncertainty, which includes the internal uncertainty and the uncertainty associated with estimating nuclide production rate. All uncertainties are reported at  $\pm 1\sigma$ .

**Supplementary Table 3. Deviations between  $^{10}\text{Be}$  age and deglaciation age.**

Sample ID <sup>a</sup>	Latitude (deg.)	Longitude (deg.)	$^{10}\text{Be}$ Age (kyr)	$^{10}\text{Be}$ Age Unc. (kyr)	Deglaciation Age [this study] (kyr)	Deglaciation Age [ref.16] (kyr)	Deviation [this study] (kyr)	Deviation [ref.16] (kyr)
P1	66.9564	19.7888	8.85	0.59	9.98	10.07	-1.13	-1.22
P1*	66.9564	19.7888	8.72	0.64	9.98	10.07	-1.26	-1.35
P2	66.9563	19.7903	9.68	1.19	9.98	10.07	-0.29	-0.39
P2*	66.9563	19.7903	9.93	0.61	9.98	10.07	-0.05	-0.14
H1	66.8670	19.8217	8.30	0.64	9.98	10.09	-1.68	-1.79
H2	66.8669	19.8190	8.97	0.68	9.98	10.09	-1.00	-1.11
H3	66.8668	19.8182	10.27	0.65	9.98	10.09	0.30	0.19
H4	66.8667	19.8177	8.94	0.64	9.98	10.09	-1.04	-1.14
H5	66.8672	19.8174	10.38	0.77	9.98	10.09	0.41	0.30
B1	65.9048	19.9802	20.33	1.09	10.03	10.22	10.29	10.11
B2	65.9055	19.9823	11.25	0.85	10.03	10.22	1.21	1.03
K1	65.3196	20.1246	15.75	1.36	10.09	10.27	5.66	5.48
V1	64.8704	18.7235	9.74	0.84	10.08	10.27	-0.34	-0.53
U1	64.6540	18.4866	15.44	0.98	10.09	10.29	5.35	5.15
U2	64.6544	18.4874	9.19	0.60	10.09	10.29	-0.90	-1.10
M1	63.2414	15.2392	8.38	0.65	10.12	10.37	-1.73	-1.98
M2	63.2409	15.2416	10.78	1.00	10.12	10.37	0.67	0.41

a. Duplicate measurements (i.e., two separate aliquots measured from the same sample) are denoted by \*.

**Supplementary Table 4.**  $^{10}\text{Be}$  analyses of 26 boulder and bedrock samples indicating the last remnants of the Fennoscandian ice sheet.

Publication	Sample type	Sample ID	Latitude (deg.)	Longitude (deg.)	Altitude (m a.s.l.)	Thick. (cm)	Topo. Shielding	$^{10}\text{Be}$ Conc. (atoms/g)	$^{10}\text{Be}$ Unc. <sup>a</sup> (atoms/g)	Be AMS Standard <sup>b</sup>	AMS Lab.	$^{10}\text{Be}$ Age <sup>c,d</sup> (yr)	$^{10}\text{Be}$ Age Internal Unc. <sup>e</sup> (yr)	$^{10}\text{Be}$ Age External Unc. <sup>e</sup> (yr)
Fabel et al. (2002)	boulder	Tjuolmma-945	67.1528	18.8739	945	1	0.9998	80821	10882	NIST_Cert.	PRIME	7727	1042	1079
Fabel et al. (2002)	bedrock	Tjuolmma-930	67.1578	18.8833	930	5	0.9982	100785	15613	NIST_Cert.	PRIME	10109	1570	1612
Fabel et al. (2006)	boulder	Ult-01	67.2495	18.8499	890	5	0.96	112349	5015	NIST_30200	ANSTO	10753	481	619
Fabel et al. (2006)	boulder	Ult-02	67.2553	18.8417	887	5	0.96	317901	6761	NIST_30200	ANSTO	30658*	657	1296
Fabel et al. (2006)	boulder	OF-00-05	66.9806	17.536	970	1	0.97	129637	6768	NIST_30200	ANSTO	11095	581	706
Fabel et al. (2006)	boulder	OF-00-06	66.9806	17.536	970	1	0.98	122530	3742	NIST_30200	ANSTO	10381	318	492
Fabel et al. (2006)	boulder	OF-00-07	66.9806	17.536	970	2	0.97	182547	5455	NIST_30200	ANSTO	15772*	473	743
Fabel et al. (2006)	boulder	OF-00-08	66.9806	17.536	815	3	0.97	107914	4295	NIST_30200	ANSTO	10742	429	579
Fabel et al. (2006)	boulder	OF-00-09	66.9806	17.536	815	5	0.96	114517	4221	NIST_30200	ANSTO	11708	433	606
Fabel et al. (2006)	boulder	OF-00-10	66.9806	17.536	815	2	0.98	100934	4344	NIST_30200	ANSTO	9864	426	556
Fabel et al. (2006)	boulder	OF-00-11	66.8406	17.8596	687	2	0.98	96263	3838	NIST_30200	ANSTO	10549	422	569
Fabel et al. (2006)	boulder	OF-00-12	66.8406	17.8596	687	4	0.96	84700	4975	NIST_30200	ANSTO	9624	567	665
Fabel et al. (2006)	boulder	OF-00-14	66.8052	17.4968	920	1	0.98	115535	2924	NIST_30200	ANSTO	10225	259	452
Fabel et al. (2006)	boulder	OF-00-15	66.8052	17.4968	920	3	0.97	106756	2716	NIST_30200	ANSTO	9700	247	430
Fabel et al. (2006)	boulder	OF-00-16	66.8052	17.4968	920	3	0.97	109328	1776	NIST_30200	ANSTO	9935	162	395
Fabel et al. (2006)	boulder	OF-00-17	66.5499	17.5039	760	4	0.96	121970	4336	NIST_30200	ANSTO	13007*	464	662
Fabel et al. (2006)	boulder	OF-00-18	66.5499	17.5039	760	2	0.98	107936	4262	NIST_30200	ANSTO	11093	439	595
Fabel et al. (2006)	boulder	OF-00-19	66.5499	17.5039	760	3	0.97	130513	9033	NIST_30200	ANSTO	13669*	949	1071
Fabel et al. (2006)	boulder	99-41	66.6022	17.2333	750	3	0.97	201219	12979	NIST_Cert.	PRIME	24011*	1558	1786
Fabel et al. (2006)	boulder	99-42	66.6022	17.2333	750	2	0.98	86316	8183	NIST_Cert.	PRIME	10079	958	1025
Fabel et al. (2006)	boulder	99-43	66.6022	17.2333	750	2	0.98	141184	9396	NIST_Cert.	PRIME	16513*	1103	1256
Harbor et al. (2006)	boulder	19	67.1530	18.84185	890	0.5	0.9998	89195	13777	NIST_Cert.	PRIME	8909	1379	1416
Harbor et al. (2006)	boulder	66	67.1408	18.7667	845	3	0.9955	166806	13217	NIST_Cert.	PRIME	17804*	1417	1558
Stroeven et al. (2011)	bedrock	114	67.1273	18.75072	797	2	0.9722468	95821	4355	NIST_30200	ANSTO	9589	437	558
Unpublished data	bedrock	S-02-24	67.0045	18.28857	870	5	0.9924	84368	3433	NIST_30200	ANSTO	7953*	324	434
Unpublished data	bedrock	S-02-25	66.9038	17.83987	525	2	0.9457	62127	3465	NIST_Cert.	PRIME	9201	514	613

a. Uncertainties (Unc.) are reported at  $1\sigma$  confidence level.

b. CRONUS-Earth online calculator nomenclature. All  $^{10}\text{Be}$  concentrations (Conc.) are renormalized to standard 07KNSTD during exposure age calculations such that all results are consistent with the updated  $^{10}\text{Be}$  half-life of  $1.387 \pm 0.012$  Myr.

c. Calculated using CRONUS-Earth online calculator source code (ref.14) version 2.2 (<http://hess.ess.washington.edu/>) constants file 2.2.1 with updated reference spallation production rates (ref.15), using the time-dependent Lal/Stone scaling scheme (reference spallation production rate  $4.15 \pm 0.15$  atoms g $^{-1}$  yr $^{-1}$ ). Calculations assume density of  $2.7$  g cm $^{-3}$ .

d. Outliers for the reduced chi-square and weighted mean calculation denoted by \*.

e. Propagated errors in the chi-square and weighted mean calculation are external uncertainties, because of the different production rates at different altitudes.

## SUPPLEMENTARY REFERENCES

1. Cato, I. The definitive connection of the Swedish time scale with the present, and new date of the zero year in Döviken, northern Sweden. *Boreas* **14**, 117-122 (1985).
2. Hättestrand, C. The glacial geomorphology of central and northern Sweden. *Sveriges Geologiska Undersökning Ca* **85**, 1-47 (1998).
3. SMHA (Statens Meteorologisk-Hydrografiska Anstalt). *Förteckning över Sveriges vattenfall. Norrlands älvar från Torneälven till Natraån*. Vattenfallsstyrelsen, Norstedt Förlag, Stockholm (1930).
4. Gotthardsson, M. River discharge. National Atlas of Sweden: Climate, lakes and rivers (eds. Raab, B, and Vedin, H.) 124-129, Stockholm (1995).
5. Dunne, J., Elmore, D. & Muzikar, P. F. Scaling factors for the rates of production of cosmogenic nuclides for geometric shielding and attenuation at depth on sloped surfaces. *Geomorphology* **27**, 3-11 (1999).
6. Kubik, P.W., Christl, M. & Alfimov, V. New Primary  $^{10}\text{Be}$  standard and  $T_{1/2}$  for AMS at ETH. *Ion Beam Physics, ETH Zurich Annual report*, p. 12 (2009).
7. Nishiizumi, K., Imamura, M., Caffee, M.W., Southon, J.R., Finkel, R.C. & McAninch, J. Absolute calibration of  $^{10}\text{Be}$  AMS standards. *Nuclear Instruments and Methods in Physics Research B* **259**, 403-413 (2007).
8. Chmeleff, J., von Blanckenburg, F., Kossert, K. & Jakob, D. Determination of the  $^{10}\text{Be}$  half-life by multicollector ICP-MS and liquid scintillation counting. *Nuclear Instruments and Methods In Physics Research Section B* **268**, 192-199 (2010).
9. Korschinek, G., Bergmaierb, A., Faestermann, T., Gerstmanc, U.C., Kniea, K., Rugela, G., Wallnerd, A., Dillmann I., Dollingerb, G., Lierse von Gostomskie, Ch., Kossertf, K., Maitia, M., Poutivtseva, M. & Remmer, A. A new value for the half-life of  $^{10}\text{Be}$  by heavy ion elastic recoil detection and liquid scintillation counting. *Nuclear Instruments and Methods In Physics Research Section B* **268**, 187-191 (2010).
10. Middleton, R., Brown, L., Dezfouly-Arjomandy, B. & Klein, J. On  $^{10}\text{Be}$  standards and the half-life of  $^{10}\text{Be}$ . *Nuclear Instruments and Methods in Physics Research B* **82**, 399-403 (1993).
11. Yiou, F. & Raisbeck, G. M. Half-life of  $^{10}\text{Be}$ . *Physical Review Letters* **29**, 372-375 (1972).
12. Hofmann, H. J., Beer, J., Bonani, G., Gunten, H. R. Von, Raman, S., Suter, M., Walker, R. L., Wölfli, W. & Zimmermann, D.  $^{10}\text{Be}$ : Half-life and AMS-standards. *Nuclear Instruments and Methods In Physics Research B* **29**, 32-36 (1987).
13. Inn, K. G. W., Raman, S., Coursey, B. M., Fassett, J. D. & Walker, R. L. Development of the NBS  $^{10}\text{Be}/^{9}\text{Be}$  isotopic standard reference material. *Nuclear Instruments and Methods In Physics Research B* **29**, 27-31 (1987).
14. Balco, G., Stone, J. O., Lifton, N. A. & Dunai, T. J. A complete and easily accessible means of calculating surface exposure ages or erosion rates from  $^{10}\text{Be}$  and  $^{26}\text{Al}$  measurements. *Quaternary Geochronology* **3**, 174-195 (2008).
15. Goehring, B. M., Lohne Ø. S., Mangerud, J., Svendsen, J. I., Gyllencreutz, R., Schaefer, J. & Finkel, R. Erratum to: Late Glacial and Holocene  $^{10}\text{Be}$  production rates for western Norway. *Journal of Quaternary Science* **27**, 544 (2012).
16. Boulton, G. S., Dongelmans, P., Punkari, M. & Broadgate, M. Palaeoglaciology of an ice sheet through a glacial cycle; the European ice sheet through the Weichselian. *Quaternary Science Reviews* **20**, 591-625 (2001).